Modal Active Vibration Control of a Rotor Using Piezoelectric Stack Actuators

RICARDO C. SIMÕES
VALDER STEFFEN, JR
School of Mechanical Engineering, Federal University of Uberlândia, Building 1M, Av. João Naves de Ávila 2121, Santa Mônica, 384000-902 Uberlândia, MG, Brazil
(vsteffen@mecanica.ufu.br)

JOHAN DER HAGOPIAN
JARIR MAHFOUD
Laboratoire de Dynamique des Machines et des Structure, Institut National des Sciences Appliquées de Lyon, Bâtiment Jean d'Alembert, 8 Rue des Sciences, 69621 Villeurbanne, France

(Received 2 March 2006; accepted 28 June 2006)

Abstract: This work deals with active vibration control of a rotating machine in both steady state and transient motion. Two stacks of piezoelectric ceramic orthogonally arranged in a plane localized at one of the bearings were used as the control actuators, using a modal control strategy. The optimal controller LQR was used to calculate the control gain, working together with an LQE observer that estimates the modal state. Simulation carried out on FEM model suggested the feasibility of the control strategy, and experimental tests using a physical test rig show good agreement with the numerical results, and confirm the efficiency of the strategy.

Keywords: Optimal control, piezoelectric actuator, rotordynamics, real-time control

1. INTRODUCTION

The performance of many rotating machines is intrinsically related to their operational speed of rotation. High operational speeds can be obtained in the design of new rotors by using flexible shafts. As a consequence of this design requirement, modern machines are susceptible to high levels of vibration when working close to critical speeds, which reduce their efficiency. Moreover, mechanical vibrations are associated with fatigue, which can lead to a catastrophic failure; vibrations must, therefore, be attenuated according to international vibration standards.

One possibility is to introduce damping by using either viscoelastic materials (Dutt and Toi, 2003), or squeeze film dampers (Chu and Holmes, 2000). Passive vibration control techniques do not require the use of electronic devices and, in general, they are easy to handle and to maintain. On the other hand, their success depends on accurate knowledge

Journal of Vibration and Control, **13(1):** 45–64, 2007 DOI: 10.1177/1077546306070227

Figures 2–3, 5–19 appear in color online: http://jvc.sagepub.com

of the dynamic behavior of the machine. Additionally, passive control techniques have low versatility, i.e., any change in the machine configuration or in the loading condition may require a new damping device.

The development of microelectronics in the last three decades has allowed the implementation of active vibration control (AVC) techniques. AVC is based on a feedback control law that is applied to the mechanical system in order to obtain a suitable response. An important advantage of AVC is that it can be adjusted to suit different load conditions and machine configurations.

In the field of rotation machinery AVC can be applied either to modify the structure characteristics such as damping and stiffness (Yao et al., 1999), or to introduce a control force. The application of control forces can be achieved either directly, using actuators which correspond to fixed position forces (Barret et al., 1995), or by using an active balancing device, (Der Hagopian et al., 1999). The use of active balancing is restricted to attenuation of synchronous perturbations.

An active magnetic bearing was the first type of actuator investigated for control of rotordynamics (Schweitzer and Lange, 1976), and applies lateral forces to the rotor without contact. Burrows and Sahinkaya (1984) presented a multi-mode technique for control of a rotor. The use of magnetic bearings in high-speed rotors helps to reduce friction and mechanical wear. However, they have a number of disadvantages, notably technical complexity and continuous power consumption (Horst and Wölfel, 2004).

Hydraulic actuators can induce high control forces, allowing them to be employed on large turbomachinery in various configurations. Stanway and Burrows (1981) and Fürst and Ulbrich (1984) mounted the bearing directly on a linear hydraulic actuator. Santos (1993) placed the hydraulic actuator below the bearing pads, with the pads' position being modified by the hydraulic action. An active hydraulic bearing, based on the principle of pressurized oil injection, was also investigated by Santos (1994). However, the limitation of hydraulic devices lies in the non-linearities of hydraulic circuits. Nowadays, servo valves controlled by piezoelectric actuators can be used at frequencies of up to 550 Hz, as mentioned by Hagemeister (1999).

Piezoelectric ceramics were first used for vibration control of mechanical systems in the 1980s. Tzou (1987) showed that it is possible to control the bending modes of a flexible beam using layered piezoelectric patches. Palazzolo et al. (1989) demonstrated both by simulation and experimentally the feasibility of rotor vibration control using a stack type of piezoelectric actuators arranged on one plane. In another work, Palazzolo et al. (1993) experimented with the same type of actuators as before, but placed on two control planes. More recently, Malhis et al. (2002) controlled the vibrations of a cantilever bar by using two PZT (lead zirconate titanate) stack actuators, and demonstrated the possibility of using modal control techniques in rotating machinery applications through numerical simulation. PZT patches have also been bonded directly to the rotor shaft (Horst and Wölfel, 2002), and the transmission of the control signal performed using a slip ring. Finally, it is worth mentioning the work of Alizadeh et al. (2003) on focusing active vibration control of flexible rotors using piezo actuators, which includes experimental results obtained from a simple test rig and describes a realistic industrial application.

The high stiffness exhibited by piezoelectric stack actuators allows them to be attached directly to the bearing housing of the rotor, while their fast dynamic response, high specific force and wide broadband enable these actuators to perform high-frequency vibration

suppression in structures. Technical simplicity, ease of integrating with the structure and reasonable cost make PZT stacks very attractive compared to other types of actuator, such as the magnetic bearings.

Control of the dynamic behavior of structures can be obtained using modal control techniques, as shown by Lalanne et al. (1983), Meirovitch (1992), and Inman (2001). A modal controller is generally represented in the form of a fixed gain matrix obtained by using optimal control techniques such as LQR (Linear Quadratic Regulator), LQG (Linear Quadratic Gaussian), or robust controllers such as H_2 or H_∞ (Ogata, 1990).

The solution of LQR control problems relies on the use of a control effort that minimizes a quadratic performance function. For modal controllers, calculating the performance function requires derivation of the modal states and the control effort. However, the modal states cannot be obtained directly from physical measurements, and so must be estimated using state observers. The general procedure to obtain the LQE (Linear Quadratic Estimator) is very similar to the one used for the LQR, and both are related to the solution of a Ricatti equation, as explained by Kwakernaak and Sivan (1972).

This article deals with vibration control of a flexible horizontal rotor using PZT stack actuators. The efficiency of the control strategy was investigated in the following conditions: Rotor at rest, steady state motion and transient motion. The piezoelectric actuators are orthogonally mounted in a single plane localized at one of the rotor bearings. As a modal control technique was used, it was necessary to obtain a reduced finite element model of the system using a pseudo-modal technique. An optimal LQR controller associated with a state estimator LQE was used. First, numerical simulations are presented to check the control strategy. This is followed by a description of the controller's experimental validation. Numerical and experimental results are compared for several operating conditions, and finally our conclusions are presented.

2. THEORETICAL BACKGROUND

2.1. Rotor Equations of Motion

The equation that describes the dynamic behavior in transient motion, modeled by the Finite Element Method (FEM), is given in matrix form by:

$$[M]\left\{\ddot{\delta}\right\} + \left[D_S + \dot{\phi}G\right]\left\{\dot{\delta}\right\} + \left[K_S + \ddot{\phi}K_2\right]\{\delta\} = F_{ext} \tag{1}$$

where M is the inertia matrix, D_S is the damping matrix of the system, G is the gyroscopic matrix, K_S is the stiffness matrix, K_2 is a stiffness matrix resulting from the transient motion, δ is the system nodal displacement and F_{ext} is the vector of external forces. These matrices were presented in detail by Lalanne and Ferraris (1998).

In classical FEM, the rotor is composed of the following elements: Rigid discs with only kinetic energy, flexible shafts exhibiting both kinetic and strain energy, and bearings with elastic and dissipation characteristics. The shaft, is represented by a Timoshenko beam element with two nodes, each node having 4 degrees of freedom; two displacements and two rotations.

The pseudo-modal technique is used to reduce the dimensionality of the finite element model. The goal is to control the first m modes of the system ($m < N$, N being the total number of degrees of freedom). The reduction is achieved by changing from the physical coordinates δ to modal coordinates q:

$$\delta = \mathbf{\Phi} q \tag{2}$$

where $\mathbf{\Phi}$ is the modal basis, which contains the m first modes of the non-gyrocopic conservative associated system.

Substituting equation (2) into equation (1) and multiplying the resulting expression by $\mathbf{\Phi}^T$, the reduced equation of motion for the system can be written as:

$$\left[\tilde{M}\right]\{\ddot{q}\} + \left[\tilde{D}_S + \dot{\phi}\tilde{G}\right]\{\dot{q}\} + \left[\tilde{K}_S + \ddot{\phi}\tilde{K}_2\right]\{q\} = \tilde{F}_{ext} \tag{3}$$

where

$$\begin{aligned} \left[\tilde{M}\right] &= \mathbf{\Phi}^T[M]\mathbf{\Phi}, \quad \left[\tilde{D}_S\right] = \mathbf{\Phi}^T[D_S]\mathbf{\Phi}, \quad \left[\tilde{G}\right] = \mathbf{\Phi}^T[G]\mathbf{\Phi}, \\ \left[\tilde{K}_S\right] &= \mathbf{\Phi}^T[K_S]\mathbf{\Phi}, \quad \left[\tilde{K}_2\right] = \mathbf{\Phi}^T[K_2]\mathbf{\Phi}, \quad \text{and} \quad \tilde{F}_{ext} = \mathbf{\Phi}^T F_{ext}. \end{aligned}$$

As it is necessary to represent the dynamic behavior of the system from the control point of view, the rotor equations of motion are now rewritten in the space state form as follows:

$$\{\dot{X}\} = [A]\{X\} + [B]\{u\} \tag{4-a}$$

$$\{Y\} = [C]\{X\} \tag{4-b}$$

X being the state vector, Y the system output vector, u the vector of excitation and control, A the dynamic system matrix, B the input system matrix and C the output system matrix. Equation (4-a) can be developed to give

$$\begin{Bmatrix} \dot{q} \\ \ddot{q} \end{Bmatrix} = \begin{bmatrix} 0 & I \\ -\tilde{M}^{-1}\left(\tilde{K}_S + \ddot{\phi}\tilde{K}_2\right) & -\tilde{M}^{-1}\left(\tilde{D}_S + \dot{\phi}\tilde{G}\right) \end{bmatrix} \times \begin{Bmatrix} q \\ \dot{q} \end{Bmatrix} + \begin{bmatrix} 0 & 0 \\ -\tilde{M}^{-1} & -\tilde{M}^{-1} \end{bmatrix} \cdot \begin{Bmatrix} f_c \\ f_p \end{Bmatrix} \tag{5}$$

where I is the identity matrix, $f_c = \mathbf{\Phi}^T F_c$ and $f_p = \mathbf{\Phi}^T F_p$ are the control force and the perturbation force in modal coordinates, respectively.

2.2. Optimal Control Strategy

The aim of this work is to control the first four bending modes of the rotor-bearing system. As only a limited number of actuators and sensors are usually available, it is necessary to use a modal control strategy acting only on the target modes. The control strategy is based

on the estimation of the modal states, using the measured displacements of the rotor as the basis from which the control forces are calculated.

A digital linear quadratic regulator is used to perform the optimal control of the system. From a practical point of view, for the control implementation, it is necessary to describe the system using discrete equations, as follows:

$$\{X\}_{k+1} = [A_d]\{X\}_k + [B_d]\{u\}_k \tag{6-a}$$

$$\{Y\}_k = [C_d]\{X\}_k \tag{6-b}$$

$$[A_d] = e^{[A]\Delta t} \tag{7}$$

$$[B_d] = [A]^{-1}\left[e^{[A]\Delta t} - [I]\right][B] \tag{8}$$

$$[C_d] = Ce^{[A]\Delta t} \tag{9}$$

where Δt is the discrete time interval.

Given the system described by equation (6-a), the optimal control problem is defined as finding the control input, u_c, in equation (10), which minimizes the cost function given by equation (11).

$$\{u_c\}_k = -[K]\cdot\{X\}_k \tag{10}$$

$$J = \sum_{k_{init}=0}^{k_{fin}-1}\left(\{X\}_k^T\cdot[Q]\cdot\{X\}_k + \{u\}_k^T\cdot[R]\cdot\{u\}_k\right) \tag{11}$$

where Q is a positive definite or semi-definite real symmetric weighting matrix relating the relative importance of each state of the system, and R is a positive definite real symmetric matrix that relates the energy consumption of the actuators in performing the control.

The matrix K that solves the optimal control problem is given by:

$$[K] = \left([R] - [B_d]^T\cdot[S]\cdot[B_d]\right)^{-1}\cdot[B_d]^T\cdot[S]\cdot[A_d] \tag{12}$$

where S is a positive definite matrix obtained by solving the Riccati equation:

$$[A_d]^T\cdot[S]\cdot[A_d] - S - \left([A_d]^T\cdot[S]\cdot[B_d]\right)\cdot \left([R] + [B_d]^T\cdot[S]\cdot[B_d]\right)^{-1}\cdot\left([B_d]^T\cdot[S]\cdot[A_d]\right) + [Q] = 0 \tag{13}$$

2.3. Reconstruction of Modal States

In the present work, the control is generated from the modal state of the system. As the modal state of the system cannot be measured directly, it must be reconstructed from measurements and control history (Gaudiller and Der Hagopian, 1996). Consequently, it is necessary to

define state observers such that the reconstructed state is optimal in the sense that the mean square reconstruction error is minimized. The state reconstruction problem can be formulated as follows:

$$\{X\}_{k+1} = [A_d]\{X\}_k + [B_d]\{u\}_k + \{w_1\}_k \quad (14\text{-a})$$

$$\{Y\}_k = [C_d]\{X\}_k + \{w_2\}_k \quad (14\text{-b})$$

where w_1 and w_2 are vectors of stochastic noise related to the state variable and sensor measurements, respectively. The state variables can be estimated using the equation

$$\left\{\hat{X}\right\}_{k+1} = [A_d]\left\{\hat{X}\right\}_k + [B_d]\{u\}_k + [L]\left(\{y\}_k - [C_d]\left\{\hat{X}\right\}_k\right) \quad (15)$$

where L is the optimal observer gain matrix, which is obtained, using equation (16), by a procedure similar to the one used to obtain the gain matrix of the controller.

$$[L]_k = \left([A_d]\cdot[S_E]_k\cdot[C_d]^T\right)\cdot\left([R_E] + [C_d]\cdot[S_E]_k\cdot[C_d]^T\right)^{-1}. \quad (16)$$

Similarly, S_E is obtained through the solution of the Riccati equation

$$[S_E]_{k+1} = [A_d]\cdot[S_E]_k\cdot[A_d]^T - \left([A_d]\cdot[S_E]_K\cdot[C_d]^T\right) \times \left([R_E] + [C_d]\cdot[S_E]_k\cdot[C_d]^T\right)^{-1}\cdot\left([C_d]\cdot[S_E]_k\cdot[A_d]^T\right) + [Q_E] \quad (17)$$

where Q_E and R_E are weighting matrices defined by

$$Q_E = E\left(\{w_1\}\cdot\{w_1\}^T\right) \quad (18\text{-a})$$

$$R_E = E\left(\{w_2\}\cdot\{w_2\}^T\right) \quad (18\text{-b})$$

$$0 = E\left(\{w_1\}\cdot\{w_2\}^T\right) \quad (18\text{-c})$$

E denotes the expected value operator.

Figure 1 gives an overview of the controller. The integral feedback gain was applied to the cage displacement to guarantee static stability.

3. CONTROL IMPLEMENTATION AND VALIDATION

3.1. Rotor Test Rig Design

Figure 2 shows the model of the rotor test rig used in the present work. The horizontal flexible shaft contains two rigid disks and is supported at the ends by bearings (the left hand support is a ball bearing and the right hand one is a roller bearing). An electrical motor that can accelerate the rotor up to 6000 rpm drives the system. Table 1 presents the properties of the rotor-bearing system. The mass and thickness of the discs are 10.00 Kg and 0.029 m for D_1, and 2.00 Kg and 0.03 m for D_2. The shaft diameter is 0.04 m.

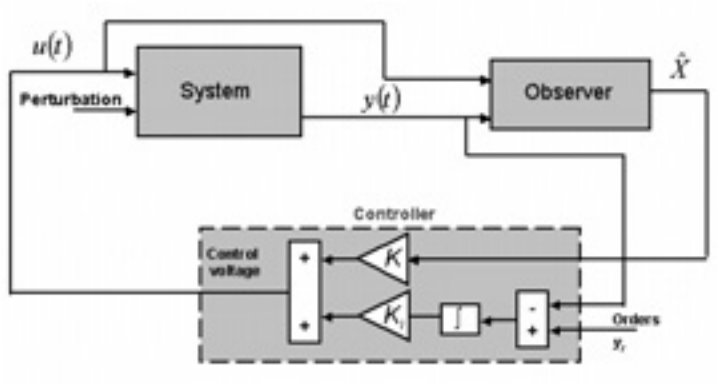

Figure 1. Control overview.

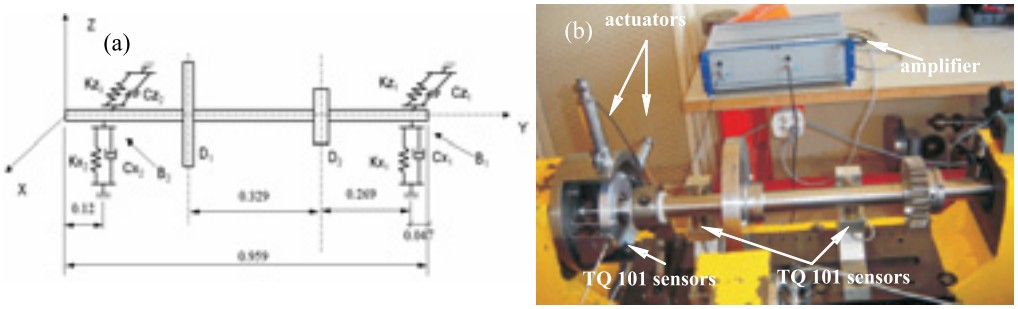

Figure 2. Test rig: (a) Model representation, (b) experimental test rig.

Table 1. Properties of the bearings.

Properties	Value
Kx_1	$3.5 * 10^6$ [N/m]
Kz_1	$8.0 * 10^6$ [N/m]
Kx_2	$8.7 * 10^6$ [N/m]
Kz_2	$6.9 * 10^6$ [N/m]

B_2 is the active bearing. It is composed of a roller bearing located in an external cage, as shown in Figure 2. This cage is attached to the chassis structure by three flexible steel beams (55.0mm length, ϕ 5.2 mm). The bending stiffness K_b of this arrangement was determined experimentally to be 1.42×10^6 N/m by performing a static deformation test.

Two PZT stack actuators fixed to the external cage provide active control. To connect the actuators to the cage, cylindrical steel stems (15.0mm length, ϕ 1.2 mm) were used in such a way that one end of each stem was bonded to the cage and the other end was bonded to the free end of the actuator, as shown in Figure 3.

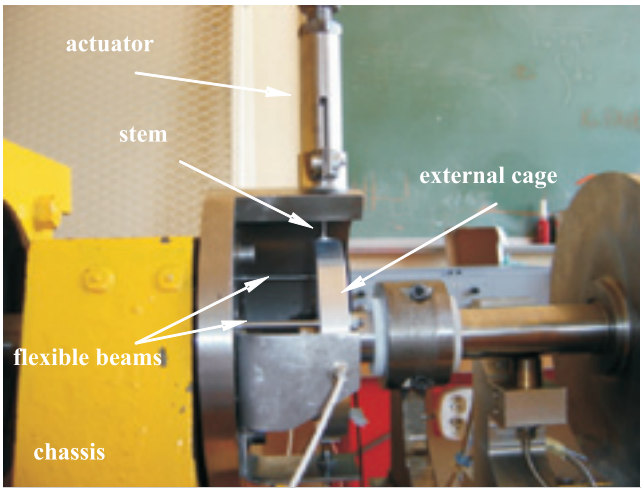

Figure 3. Active bearing.

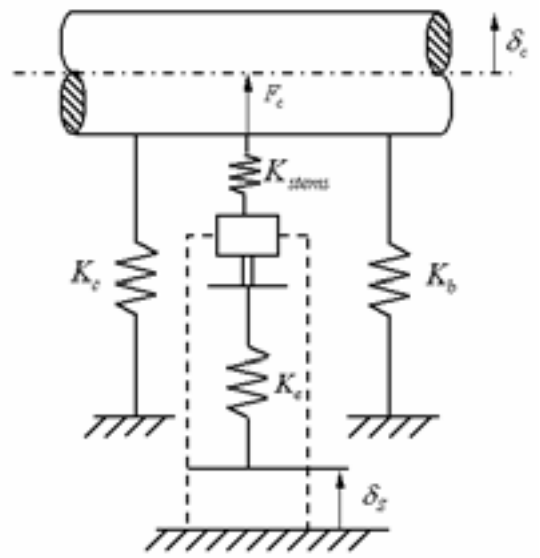

Figure 4. Active bearing scheme.

By using current experimental modal analysis techniques, the stiffness of the actuator K_a was determined to be 2.04 x 10^7 N/m.

As the stems are mounted in series with the PZT actuators (see Figure 4), the stiffness of the set stems-actuators can be represented by an equivalent stiffness K_{eq}. Thus, the control force acting on the external cage is

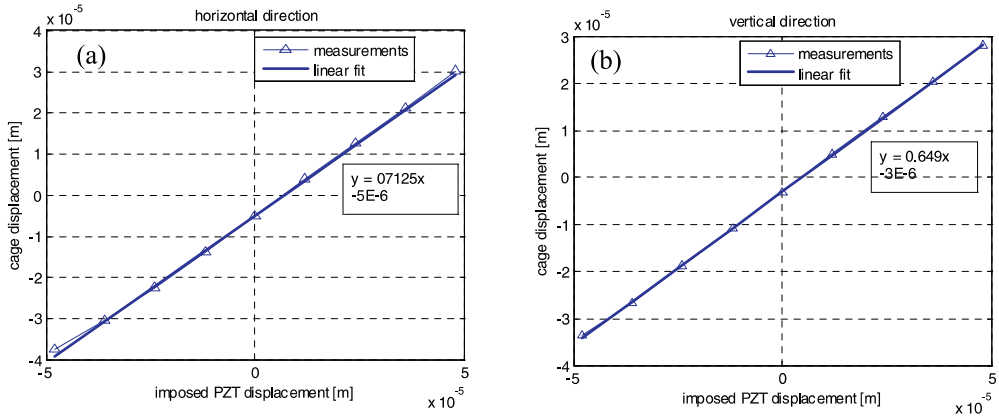

Figure 5. Results of static deformation tests in the active bearing: (a) X direction, (b) Z direction.

$$F_c = K_{eq} \cdot \delta_S \tag{19}$$

where δ_s is the displacement imposed in the base of PZT stack, which is a function of the voltage V:

$$\delta_S = \alpha \cdot G_a \cdot V. \tag{20}$$

Where α is the piezoelectric coefficient (1.2×10^{-7} m/V) and G_a is the gain of the voltage amplifier (100).

K_{eq} was determined using a static deformation test. A constant voltage was applied to the stack actuator to obtain the imposed displacement given by equation (20), and the displacement δ_c of the cage was measured by a position sensor. At the static equilibrium condition, the imposed displacement of the PZT actuator and the measured cage displacement are related to the stiffness values by the equation

$$\frac{\delta_c}{\delta_S} = \frac{K_{eq}}{K_{eq} + K_b + K_c} \tag{21}$$

where K_c is the bending stiffness (1.5×10^6 N/m) of the coupling that connects the rotor to the electrical motor. Figures 5(a) and (b) show the experimental results for the static deformation test along the X and Z directions, respectively. From equation (21), it is possible to obtain the equivalent stiffness along the horizontal and vertical directions (7.2×10^6 N/m and 5.4×10^6 N/ m, respectively). To calculate the stiffness values of the active bearing, one must add K_b to K_{eq}.

3.2. Rotor Finite Element Model

A FEM model of the rotor was used to carry out numerical simulations and to determine both the control and the observer gain matrices that were used in the experimental implementation

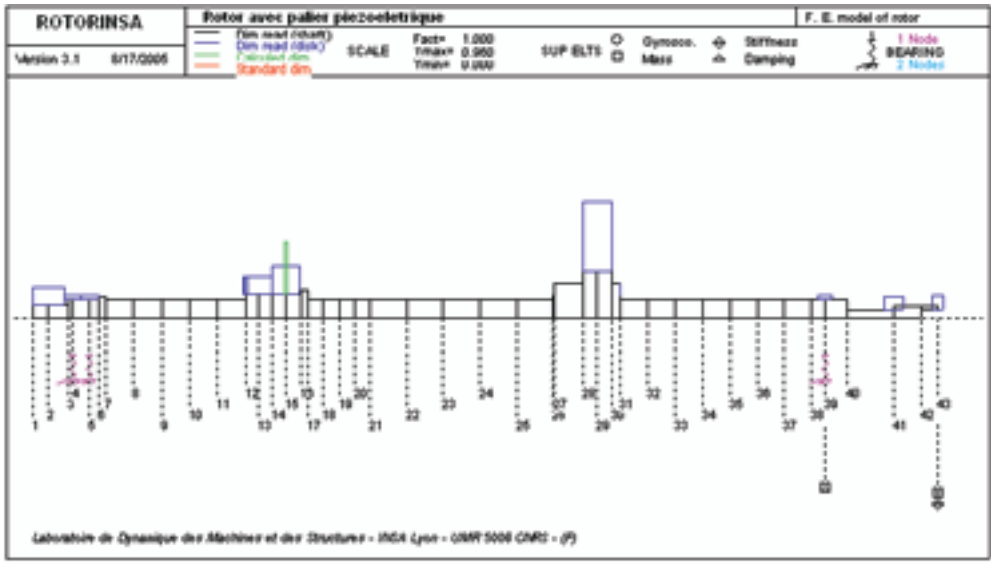

Figure 6. Model meshing.

Table 2. Modal characteristics of the rotor-bearings model.

Mode	Direction	Frequency	Modal damping factor
1	X	66.5	0.02
2	Z	66.8	0.02
3	X	193.1	0.01
4	Z	208.1	0.01

of the controller. The software ROTORINSA was applied to obtain the modal matrices of the rotor considering the first eight modes for system simulation purposes and the first four modes for calculation of the gain matrices. Modal damping was introduced in the model as shown in table 2. The model meshing is presented in Figure 6. The active bearing is the one located at node 39.

The calculation of both the control and the observer gain matrices were performed using Matlab. The weighting matrices for the controller and the observer are given in equations (22-a) and (22-b), respectively.

$$\begin{aligned} Q &= \mathrm{diag}\left(\begin{bmatrix} 1 & 0 & 10 & 1 & 1 & 10 & 10 & 1 & 1 \end{bmatrix}\right), \\ [R] &= \mathrm{diag}\left(\begin{bmatrix} 0.002 & 0.002 \end{bmatrix}\right) \end{aligned} \tag{22-a}$$

$$\begin{aligned} Q_e &= \mathrm{diag}\left(\begin{bmatrix} 3\cdot 10^6 & 3\cdot 10^6 & 1\cdot 10^7 & 1\cdot 10^7 & 1\cdot 10^4 & 1\cdot 10^4 & 5\cdot 10^4 & 5\cdot 10^4 \end{bmatrix}\right), \\ R_e &= \mathrm{diag}\left(\begin{bmatrix} 1 & 1 & 1 & 1 \end{bmatrix}\right) \end{aligned} \tag{22-b}$$

3.3. Experimental Setup

The experimental setup is composed of two piezoelectric actuators (Physik Instrumente P-245.70; $\pm$ 120μm; 2000N compression; 300 N traction) driven by a power amplifier (Physik Instrumente E472) with a constant gain of 100. The displacements were measured using eddy current sensors along the X and Z directions: Two (Vibrometer TQ 101) located at node 33, two (Vibrometer TQ 103) located at node 39, and two further sensors located at node 22. These last probes (node 22) were used to perform the spectral analysis of the rotor. The signal acquisition and data processing was done using Dspace cards: A calculation card (DS1005) equipped with a digital signal processor (DSP TMS320C40), a 12 bit acquisition card (DS2002) with analog to digital time conversion rate of 3.3 μs per channel, and a 12 bit restitution card (DS2101) with digital to analog time conversion rate of 3.3 μs per channel.

3.4. Results

The performance of the controller was tested for several operating conditions (rest, steady-state rotation and transient rotation) under different perturbation cases (impulsive, step and unbalance).

3.4.1. Rotor at Rest

The Bode diagrams of the rotor at rest are shown in Figure 7. The PZT stack actuators along the X and Z directions excited the system using a sinusoidal sweep signal. Measurements were performed at the position corresponding to node 22. It can be seen that the LQR controller was able to impose a vibration level reduction as large as 20 dB at the first critical speed. Due to its design characteristics, the controller is very effective at the first two critical speeds. It can be seen that the controller has no effect at frequencies significantly different to the critical speeds, however, especially those higher than the first critical speed. It is also worth noting that the vibrations in the controlled case have higher amplitudes than those in the uncontrolled case for frequencies lower than the first critical speed.

Figures 8 and 9 present the experimental and simulation results, respectively, for an impulsive force applied in the vertical direction in the position corresponding to node 29. To test the efficiency of the integral feedback, a 2V step excitation was applied to the actuators; the results for this test are shown in Figures 10 (experimental) and 11 (simulation). It can be seen that the settling time was reduced from 0.3 to 0.05 seconds.

3.4.2. Steady-state Rotation

The stability of the controller was tested with the rotor operating at a constant speed of 2000 rpm. In this case, the machine was excited by its residual imbalance and by a step excitation similar to the one used in the test at rest. As expected, the controller was effective in reducing impulsive perturbations for both X and Z directions. However, it can be seen that this type of controller is not optimized for attenuating unbalance vibrations outside the critical speed band from the results presented in Figures 12 to 15. (Although it can be seen that good correspondence exists between the simulated and experimental results.) No experimental

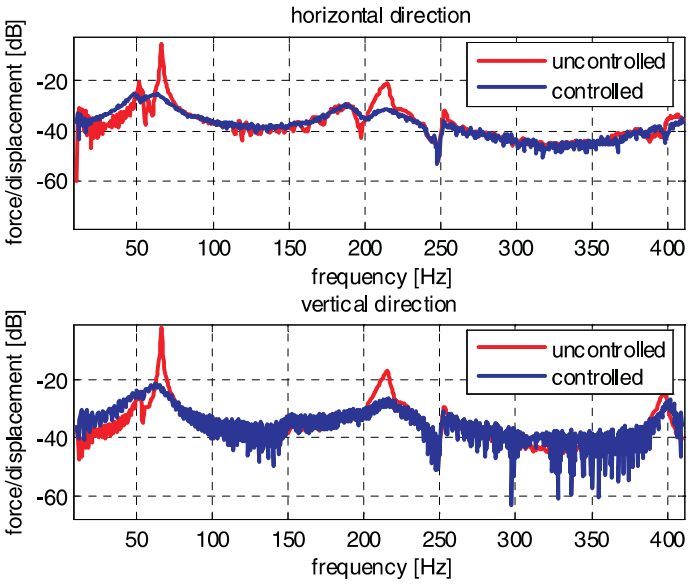

Figure 7. Experimental Bode diagram of the rotor.

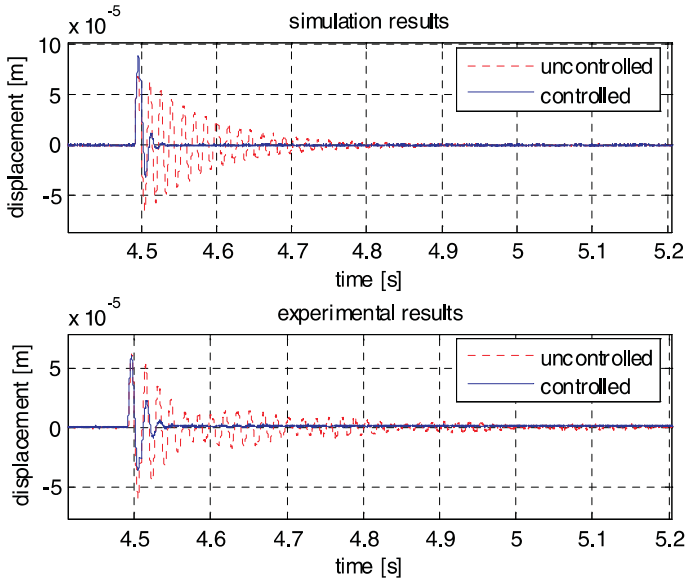

Figure 8. Time response at node 33, vertical (Z) direction.

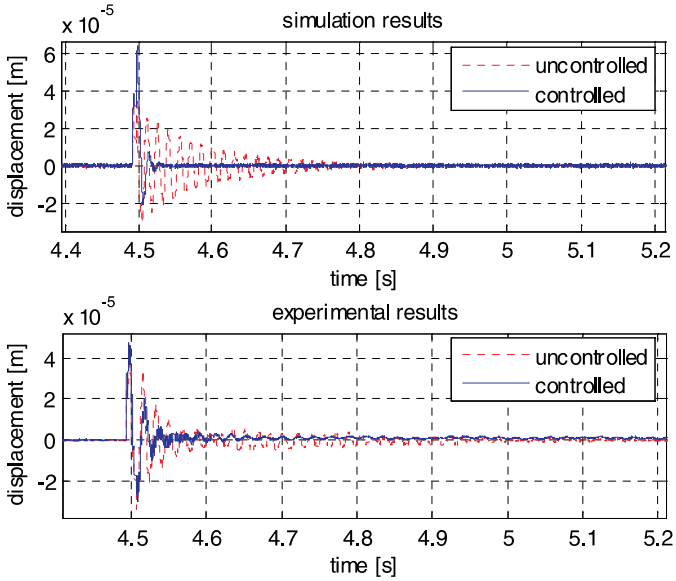

Figure 9. Time response at node 39, vertical (Z) direction.

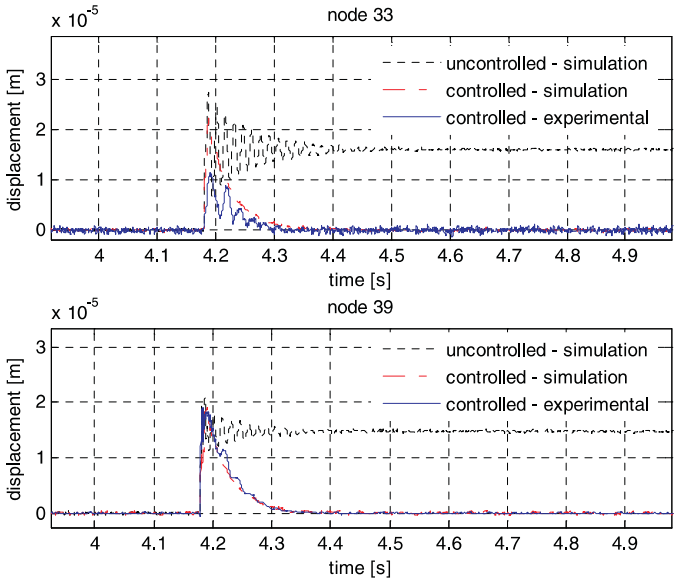

Figure 10. Time response (in the X direction) to vertical step perturbation.

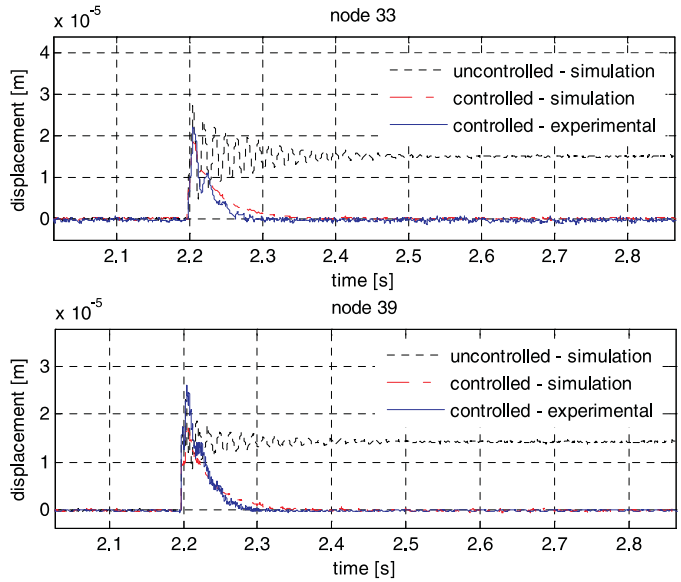

Figure 11. Time response (in the Z direction) to vertical step perturbation.

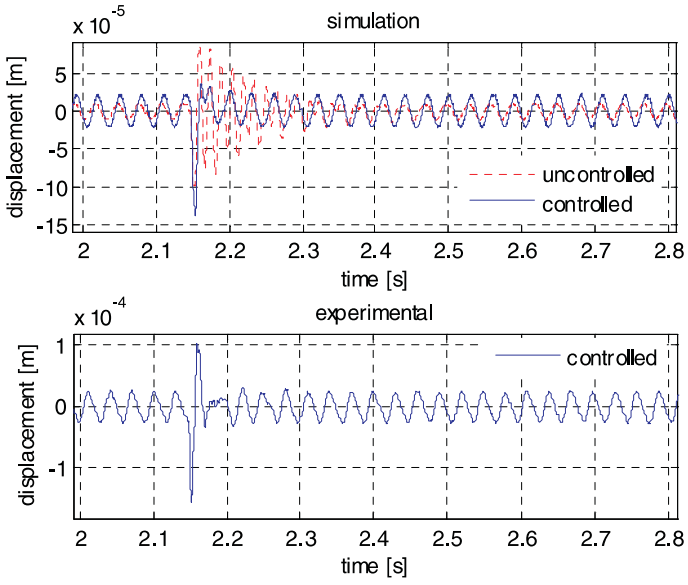

Figure 12. Time response in steady state motion at node 33, horizontal (X) direction.

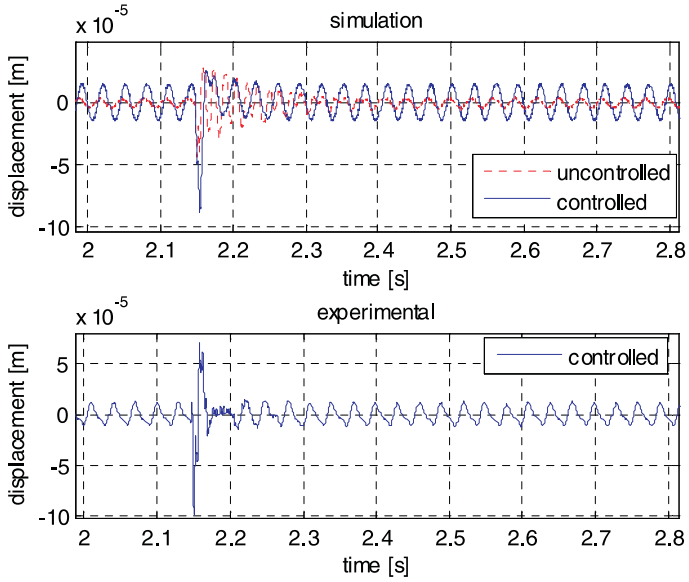

Figure 13. Time response in steady state motion at node 39, horizontal (X) direction.

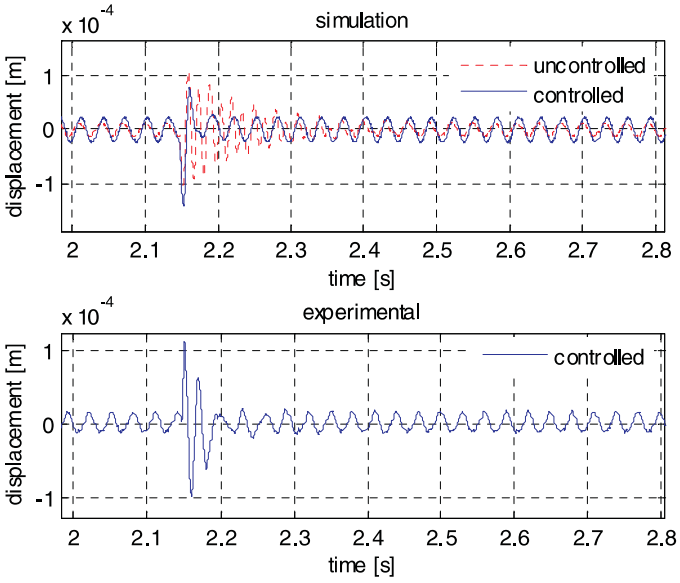

Figure 14. Time response in steady state motion at node 33, vertical (Z) direction.

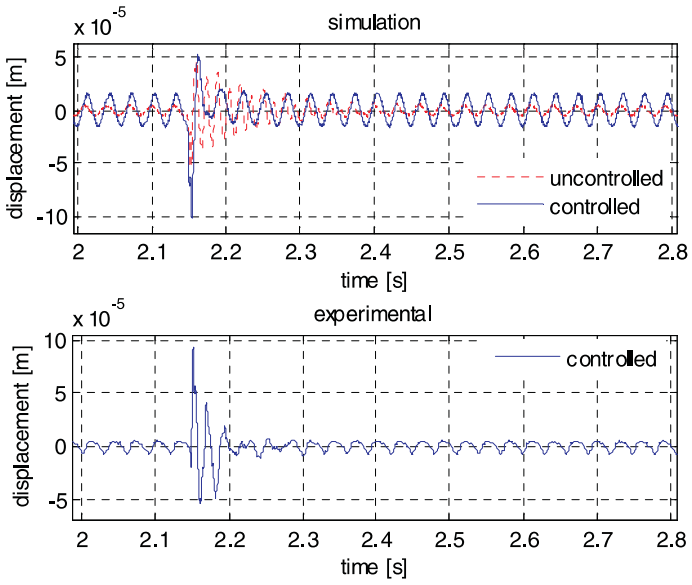

Figure 15. Time response in steady state motion at node 39, vertical (Z) direction.

results were obtained for the uncontrolled case, for safety reasons; the simulations of the uncontrolled case showed dangerous vibrations.

3.4.3. Transient Motion

The dynamic behavior of the rotor-bearing system was analyzed in the range 2400-6000 rpm. The acceleration rate used was 252 rpm/s. The controller achieved and a smooth passage through the first critical speed, as shown in Figures 16 to 19 for the X and Z directions at two different measurement points. The vibration level was reduced by a factor of approximately ten at node 33 and by a factor of four at node 39. For the uncontrolled case, the difference between experimental and simulation results is due to a sudden stiffness reduction in the active bearing when passing through the first critical speed (the stem collapses under resonance conditions). This means that the high vibration level for the uncontrolled case modifies the rigidity between the pusher and the bearing case and consequently the stiffness of the system is drastically reduced.

4. CONCLUSIONS

The goal of the present work was to explore and demonstrate the possibility of using piezoelectric actuators for vibration control in rotating machinery. The use of optimal control was selected due to its simplicity and the ease of its practical implementation.

Vibration control of a flexible horizontal rotor using PZT stack actuators was presented and assessed in both numerical simulation and experimentation. The piezoelectric actuators

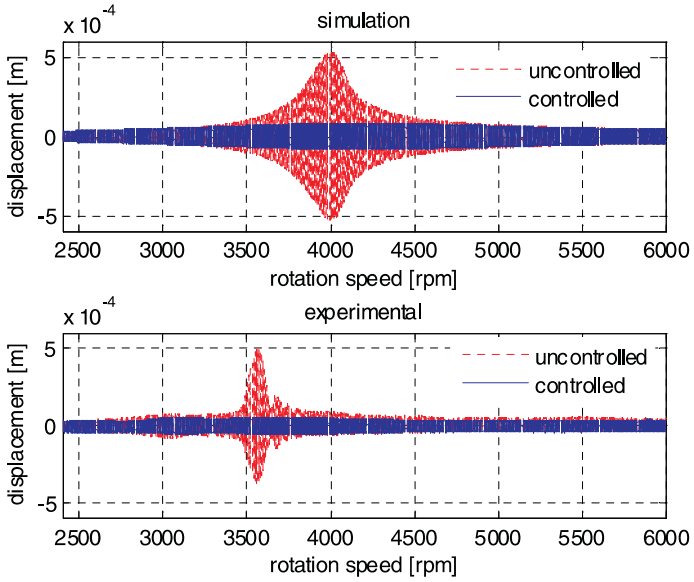

Figure 16. Time response in transient motion at node 33, horizontal (X) direction.

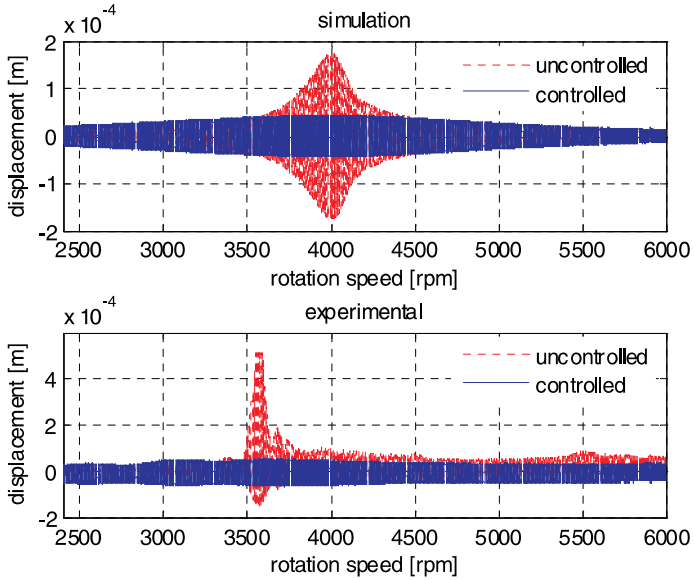

Figure 17. Time response in transient motion at node 39, horizontal (X) direction.

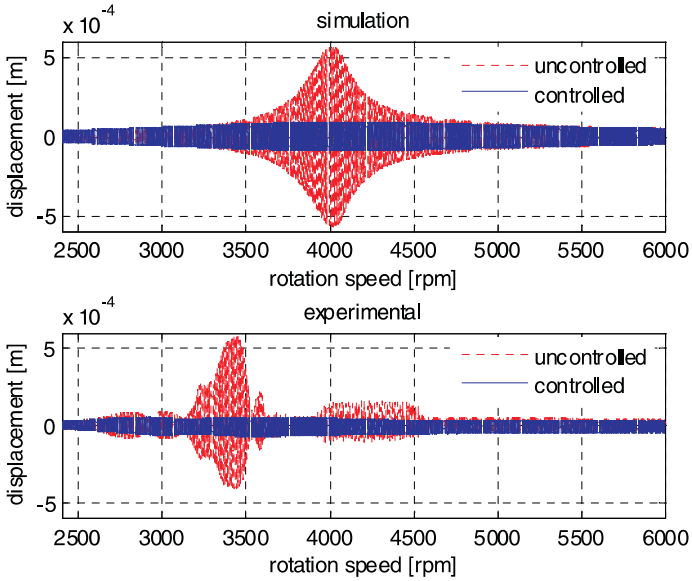

Figure 18. Time response in transient motion at node 33, vertical (Z) direction.

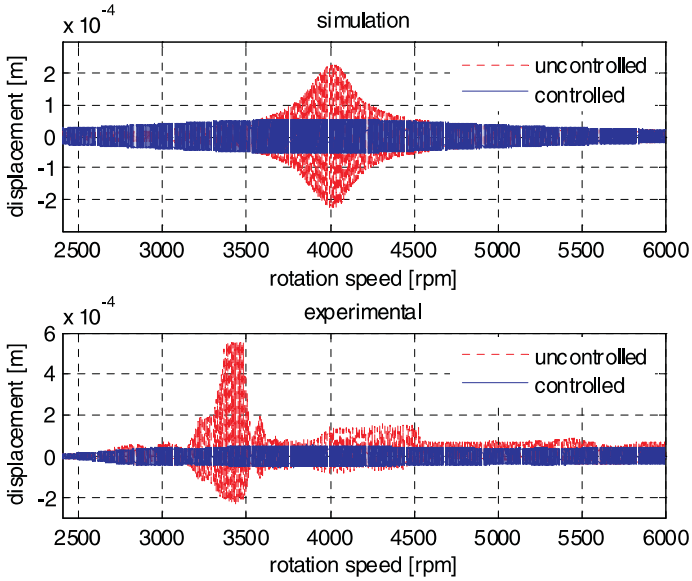

Figure 19. Time response in transient motion at node 39, vertical (Z) direction.

were mounted in a single plane localized at one of the rotor bearings. An optimal LQR controller associated with a state estimator LQE was used. A modal control technique was performed, using a reduced finite element model of the system produced with a pseudo-modal technique. The efficiency of this control strategy was demonstrated both numerically and experimentally with the rotor at rest, in steady state motion and in transient motion.

With the rotor at rest, it was observed that the controller enabled a vibration level reduction as large as 20 dB for the first critical speed, and the settling time was reduced from 0.3 to 0.05 seconds. Due to its design characteristics the controller was very effective at the first two critical speeds, but had little influence outside this range, especially at frequencies higher than the first critical speed. For frequencies lower than the first critical speed, the vibrations in the controlled case have higher amplitudes than those in the uncontrolled case. Additional research is being carried out to improve the performance of the controller under such conditions.

For steady state motion, the controller was effective in reducing impact vibrations in both the X and Z directions. Due to dangerous vibrations observed in the simulations of the uncontrolled case, no experimental tests were performed under these conditions. However, the simulation model is very representative of the rotor-bearing system, and the numerical results show significant and fast attenuation of the imposed perturbation. It is worth mentioning that the controller was effective not only at the control plane (node 39), but also at another measurement point (node 33). Thus, the controller was experimentally validated.

Finally, for transient motion it was observed that a smooth passage through the first critical speed occurred in the controlled case. The vibration level was attenuated by a factor of approximately ten at the measurement point corresponding to node 33 and a factor of four at the one corresponding to node 39. However, it is important to observe that the controller was effective over the entire analyzed rotation band.

The present work has demonstrated that a simple optimal controller can be successfully used for vibration attenuation in flexible rotors and that a single active plane is enough to provide control effort. The efficiency of the control strategy was simulated and experimentally tested with the rotor at rest, in steady state motion and in transient motion, and the mounting of the active piezoelectric actuators is simple and could easily be extended to industrial applications.

The results obtained are very encouraging in the sense that piezoelectric actuators provide significant control forces over an important frequency band. These characteristics suggest the possibility of using piezoelectric actuators for balancing purposes, and research is currently being carried out on that possibility.

Acknowledgments. The first author of this paper is thankful to CAPES Brazilian Agency for his PhD scholarship. The third author is grateful to CNPq Research Agency for his research scholarship. The fourth author is also grateful to CNPq Research Agency for his research grant.

REFERENCES

Alizadeh, A., Ehmann, C., Schönhoff, U., and Nordmann, R., 2003, "Active bearing of rotors utilizing robust controlled piezo actuators," *Proceedings of DETC'03*, Chicago, Illinois, September 2–6.

Barret, T. S., Palazzolo, A.B., and Kascak, A. F., 1995, "Active vibration control of rotating machinery using piezoelectric actuators incorporating flexible casing effects," *Journal of Engineering for Gas Turbines and Power* **117(1)**, 176–187.

Burrows, C. R. and Sahinkaya, M. N., 1984, "Vibration control of multi-mode rotor bearing systems," *Proceedings of the Royal Society of London* **386**, 77–94.

Chu, F. and Holmes, R., 2000, "The damping capacity of the squeeze film damper in suppressing vibration of a rotating assembly," *Tribology International* **33**, 81–97.

Der Hagopian, J., Gaudiller, L., Alauze, C., and Voinis, P., 1999, "Synchronous control of large shafts lines by active balancing," *Proceedings of Eurodyname'99*, Ulm, Germany, July 11–16, pp. 37–43.

Dutt, J. K. and Toi, T., 2003, "Rotor vibration reduction with polymeric sectors," *Journal of Sound and Vibration* **262** , 769–793.

Fürst, S. and Ulbrich, H., 1984, "An active support system for rotors with oil-film bearings," *ImechE International Conference on Vibrations in Rotating Machinery*, England, pp. 61–67.

Gaudiller, L. and Der Hagopian, J., 1996, "Active control of flexible structures using a minimum number of components," *Journal of Sound and Vibration* **193(3)**, 713–741.

Hagemeister, W., 1999, "Piezoelektrisch vorgesteuertes 3/3-wegeservoventil," *Ölhydraulik und Pneumatik* **43(7)**, 538–543.

Horst, H.-G. and Wölfel, H. P., 2004, "Active vibration control of a high speed rotor using PZT patches on the shaft surface," *Journal of Intelligent Material Systems and Structures* **15**, 721–728.

Inman, D. J., 2001, *Engineering Vibration*, Prentice Hall, Upper Saddle River, NJ.

Kwakernaak, H. and Sivan, R., 1972, *Linear Optimal Control Systems*, Wiley, New York.

Lalanne, M. and Ferraris, G., 1998, *Rotordynamics Prediction in Engineering*, 2nd Edition, Wiley, New York.

Lalanne, M., Berthier, P., and Der Hagopian, J., 1983, *Mechanical Vibration for Engineers*, Wiley, Chichester, UK.

Malhis, M., Gaudiller, L., and Der Hagopian, J., 2002, "Fuzzy modal control of a flexible rotor by piezoeletric actuators arranged on a plane," *Proceedings of the Sixth International Conference on Rotor Dynamics*, Sydney, Australia, September 30–October 4, Vol. 1, pp.101–108.

Meirovitch, L., 1992, *Dynamics and Control of Structures*, Wiley, New York.

Ogata, K., 1990, *Modern Control Engineering*, Prentice-Hall, New York.

Palazzolo, A. B., Jogannathan, S., Kascak, A. F., Montague, G. T., and Kiraly, L. J., 1993, "Hybrid active vibration control of rotor bearing systems using piezoelectric actuators," *Journal of Vibration and Acoustics* **115**, 111–119.

Palazzolo, A. B., Kascak, A. F., Montague, G. T., and Kiraly, L. J., 1989, "Piezoelectric Pusher for Active Vibration Control of Rotating Machinery," *Transactions of the ASME* **111**, 298–305.

Santos, I. F., 1993, *Aktive Kippsegmentlagerung-theorie und experiment*, Fortschritt-Berichte VDI reihe 11, **189**.

Santos, I.F., 1994, "Design and evaluation of two types of active tilting-pad bearings," *Proceedings of the IUTAM Symposium on Active Control of Vibration*, Bath, UK, pp. 79–87.

Schweitzer, G. and Lange, R., 1976, "Characteristics of a magnetic rotor bearing for active vibration control," *ImechE Conference on Vibration in Rotating Machinery*, Cambridge, Paper no. C239/76.

Stanway, R. and Burrows, C. R., 1981, "Active vibration control of a flexible rotor on flexible-mounted journal bearings," *ASME Journal of Dynamic Systems, Measurement and Control* **103**, 383–388.

Tzou, H. S., 1987, "Active vibration control of flexible structures via conserve piezoelectricity," *Proceedings of the 20th Midwestern Mechanics Conference*, Developments in Mechanics, Vol. 14-c, pp. 1201–1206.

Yao, G. Z., Qiu, Y., Meng, G., and Fang, T., 1999, "Vibration control of a rotor system by disk type electrorheological damper," *Journal of Sound and Vibration* **219**, 175–188.